Influenza infection triggers disease in a genetic model of experimental autoimmune encephalomyelitis

Stephen Blackmore[a], Jessica Hernandez[a], Michal Juda[a], Emily Ryder[b], Gregory G. Freund[a,c], Rodney W. Johnson[a,b,d], and Andrew J. Steelman[a,b,d,1]

[a]Department of Animal Sciences, University of Illinois Urbana–Champaign, Urbana, IL 61801; [b]Neuroscience Program, University of Illinois Urbana–Champaign, Urbana, IL 61801; [c]Department of Pathology, University of Illinois Urbana–Champaign, Urbana, IL 61801; and [d]Division of Nutritional Sciences, University of Illinois Urbana–Champaign, Urbana, IL 61801

Edited by Lawrence Steinman, Stanford University School of Medicine, Stanford, CA, and approved June 13, 2017 (received for review December 13, 2016)

Multiple sclerosis (MS) is an autoimmune disease of the central nervous system. Most MS patients experience periods of symptom exacerbation (relapses) followed by periods of partial recovery (remission). Interestingly, upper-respiratory viral infections increase the risk for relapse. Here, we used an autoimmune-prone T-cell receptor transgenic mouse (2D2) and a mouse-adapted human influenza virus to test the hypothesis that upper-respiratory viral infection can cause glial activation, promote immune cell trafficking to the CNS, and trigger disease. Specifically, we inoculated 2D2 mice with influenza A virus (Puerto Rico/8/34; PR8) and then monitored them for symptoms of inflammatory demyelination. Clinical and histological experimental autoimmune encephalomyelitis was observed in ∼29% of infected 2D2 mice. To further understand how peripheral infection could contribute to disease onset, we inoculated wild-type C57BL/6 mice and measured transcriptomic alterations occurring in the cerebellum and spinal cord and monitored immune cell surveillance of the CNS by flow cytometry. Infection caused temporal alterations in the transcriptome of both the cerebellum and spinal cord that was consistent with glial activation and increased T-cell, monocyte, and neutrophil trafficking to the brain at day 8 post infection. Finally, *Cxcl5* expression was up-regulated in the brains of influenza-infected mice and was elevated in cerebrospinal fluid of MS patients during relapse compared with specimens acquired during remission. Collectively, these data identify a mechanism by which peripheral infection may exacerbate MS as well as other neurological diseases.

upper-respiratory viral infection | multiple sclerosis | neuroinflammation | immune cell surveillance | experimental autoimmune encephalomyelitis

The bidirectional connectivity between the brain and the immune system is well-established. It has been repeatedly demonstrated that systemic inflammation brought on by activation of toll-like receptors (TLRs) on cells in the periphery can trigger glial activation in mice and humans (1–3). Furthermore, upper-respiratory infection with influenza A (4, 5) and porcine reproductive and respiratory syndrome viruses up-regulate proinflammatory cytokines within the CNS and cause alterations to the microglial sensome (6). Under normal physiological circumstances, activation of glial cells by peripheral inflammatory processes likely facilitate functions that are essential for the maintenance of homeostasis. For example, type I IFN signaling to brain endothelial cells contributes to the development of sickness behaviors in rodents, which are important for combating infection (7). Furthermore, systemic inflammation-induced glial activation promotes immune surveillance of the CNS (2, 8). The function of this surveillance is not entirely clear, but may serve to protect against infection of the CNS parenchyma and under certain circumstances facilitate repair (9). Conversely, aberrant neuroinflammation contributes to the pathogenesis of a myriad of neurological diseases and T-cell extravasation into the CNS is not always beneficial. Intriguingly, systemic inflammation brought on by pathogenic infection can exacerbate neuroinflammatory processes and may affect the progression of many neurological diseases including Alzheimer's disease (10, 11), Parkinson's disease (12), and multiple sclerosis (13–17).

We are interested in determining how upper-respiratory infection contributes to the progression of neurological diseases including multiple sclerosis (MS), the most prominent autoimmune-mediated demyelinating and neurodegenerating disease of the CNS. The majority of MS patients exhibit an oscillating disease course that is characterized by relatively short periods of neurological dysfunction followed by periods of remission, termed relapsing-remitting MS (18). Importantly, both relapse rate and intervals between relapses are predictors of disability outcome and relapses contribute to the development of permanent neurological dysfunction (19). Interestingly, within 5 weeks of contracting an upper-respiratory infection an estimated 27–41% of patients will suffer disease exacerbation (13, 15, 16, 20–22). In addition, some reports suggest that relapses occurring around the time of infection are associated with sustained neurological deficits, increased relapse severity, and an increased number of gadolinium-enhancing lesions as measured by MRI (21). Picornaviruses have been identified as triggers of relapse (13, 23), but infection with other viruses, including influenza A virus, has also been associated with exacerbated disease (24). These data suggest that upper-respiratory infection with viral pathogens can precipitate relapse, but the mechanisms remain poorly defined.

In the case of MS patients, it is possible that upper-respiratory infection-induced glial activation triggers immune surveillance

Significance

Peripheral infections exacerbate symptoms of many neurological diseases, including the most common autoimmune demyelinating disease of the central nervous system (CNS), multiple sclerosis (MS). We demonstrate that influenza viral infection of autoimmune-prone mice triggers clinical and histological disease. We further show that influenza infection alters the transcriptome of the central nervous system and facilitates immune cell trafficking to the brain. Finally, we identified a specific chemokine that is upregulated in the CNS during infection that is also increased in the cerebrospinal fluid of MS patients during relapse. These observations improve our understanding of how peripheral infection may act to exacerbate neurological diseases such as multiple sclerosis.

Author contributions: A.J.S. designed research; S.B., J.H., M.J., E.R., G.G.F., and A.J.S. performed research; G.G.F., R.W.J., and A.J.S. contributed new reagents/analytic tools; S.B., J.H., M.J., E.R., and A.J.S. analyzed data; and S.B. and A.J.S. wrote the paper.

The authors declare no conflict of interest.

This article is a PNAS Direct Submission.

Data deposition: The sequence reported in this paper has been deposited in the NIH Gene Expression Omnibus database (accession no. GSE96870).

[1]To whom correspondence should be addressed. Email: asteelma@illinois.edu.

This article contains supporting information online at www.pnas.org/lookup/suppl/doi:10.1073/pnas.1620415114/-/DCSupplemental.

of the CNS that may be detrimental. To model the effects of upper-respiratory infection on relapse and/or disease progression in MS patients, we infected autoimmune-prone T-cell receptor transgenic (2D2) mice with mouse-adapted human influenza A virus. This strategy was chosen because, although ~90% of $CD4^+$ T-cells in 2D2 mice express a T-cell receptor (TCR) with specificity for myelin oligodendrocyte glycoprotein (MOG_{35-55}) and neurofilament-m ($NF\text{-}M_{18-30}$), few (4%) develop spontaneous classic experimental autoimmune encephalomyelitis (EAE) (25). Additionally, the presence of circulating autoreactive cells enabled us to bypass the need to polarize and activate T-cells before injection. Finally, influenza A virus can induce glial activation (4, 5) and has been associated with increased relapse risk in MS patients (22, 24, 26). Here, we report that upper-respiratory infection with influenza virus is capable of causing neurological disease in 2D2 mice. Furthermore, we found that viral infection alone caused temporal transcriptomic changes to the cerebellum and spinal cord that were in part mediated by IFN signaling. Finally, we demonstrate that infection caused immune cell surveillance of the CNS.

Results

Influenza A Infection Causes EAE Onset in 2D2 Mice. Transgenic 2D2 mice possess an inherent reduction in $CD8^+$ T-cells that might impede virus-specific immune responses (25). Indeed, following intranasal inoculation with a normally nonlethal dose of influenza [1.0 hemagglutinating unit (HAU)], 2D2 mice lost more weight, and a higher percentage succumbed to infection compared with controls (Fig. S1 *A* and *B*). However, 2D2 mice that were inoculated with a lower viral titer (0.7 HAU) had substantially reduced mortality rates.

Approximately 29% of virus-inoculated 2D2 mice developed clinical signs of EAE within 2 wk of infection. In contrast, neither saline-inoculated C57BL/6 nor 2D2 mice developed signs of disease. This incidence is similar to the effect of upper-respiratory infection on relapse in MS and is significantly higher than would be anticipated to occur in this strain (χ^2 = 37.565; $P < 0.001$). Importantly, viral *M1* was not detectible in the olfactory bulbs, cerebellum, or spinal cords of infected 2D2 mice at day 8 post infection (p.i.). Maximal disease severity of influenza-induced EAE ranged from tail weakness to unilateral paralysis (Table 1). Histopathological analysis confirmed the presence of inflammation and demyelination in the spinal cord and cerebellum of influenza-infected 2D2 mice (Fig. 1 *A* and *B*). We did not observe demyelination in control mice. To determine if influenza inoculation caused autoreactive T-cell trafficking to the CNS, we measured the percentages of $CD45^+V\alpha3.2^+$ isolated from influenza-inoculated 2D2 mice, of which 3/5 had mild signs of EAE (tail paresis with wobble; score of 1), and control 2D2 mice. Influenza increased percentages of both $CD45^+V\alpha3.2^+$ autoreactive T-cells and $CD45^{hi}V\alpha3.2^-$ cells in the brains of infected mice (Fig. 1*C*). Together, these data indicate that upper-respiratory infection is capable of triggering moderate signs of EAE in T-cell receptor transgenic 2D2 mice.

Table 1. Effect of influenza infection on neurological signs of EAE

Genotype	Inoculum	Incidence	Percent	Maximum score*	Day of onset*
C57BL/6	FLU	0/5	0	NA	NA
2D2	Saline	0/13	0	NA	NA
2D2	FLU	7/24	29	2	10

FLU, influenza; NA, not applicable.
*Represents the median value. Results are from four independent experiments.

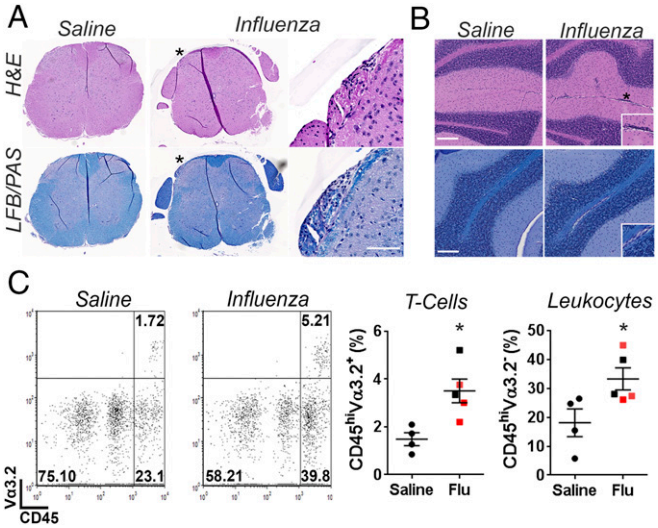

Fig. 1. CNS pathology in saline- and influenza-infected 2D2 mice. (*A* and *B*) Transgenic 2D2 mice were inoculated with saline (n = 5) or influenza (n = 8; 0.7 HAU). After 28 d post infection, mice were euthanized. Brains and spinal cord sections were stained with H&E to identify inflammation and Luxol Fast Blue and periodic acid Schiff (LFB/PAS) to identify demyelination. Sections were scanned by a rater blinded to condition. (*A*) Spinal cord lesion showing inflammation (*Top*) and demyelination (*Bottom*) in an influenza-infected mouse. (*Right*) Higher magnification of lesion is denoted by an asterisk. (Scale bar is 50 μm.) (*B*) Representative cerebellar H&E (*Top*) and LFB/PAS (*Bottom*) stain showing perivascular cuffing and demyelination (*) in influenza but not in saline-inoculated mice. (Scale bar is 250 μm.) *Insets* have been magnified 20×. (*C*) Transgenic 2D2 mice were inoculated with saline (n = 4) or influenza (n = 5; 0.7 HAU). The brains were extracted from control and influenza-infected mice at day 8 and from three influenza-infected mice that developed mild signs of EAE (scores of 0.5–1) at day 11 p.i. and then processed for flow cytometry. All events were initially gated on viable and single cells (Fig. S2). Representative flow plots showing autoreactive T-cells ($CD45^{hi}V\alpha3.2^+$) (*Left*). The percentages of autoreactive T-cells and leukocytes ($CD45^{hi}V\alpha3.2^-$) from the brains of saline- and influenza-inoculated mice are presented (*Right*). Influenza-infected mice with symptoms of EAE are represented by red squares. Results are means ± SE; *$P < 0.05$.

Infection Causes Alterations to the Cerebellar and Spinal Cord Transcriptome. To gain further insight into how peripheral infection may cause EAE and might act to exacerbate other neurological diseases, we examined transcriptomic changes to the cerebellar and spinal cord tissues isolated from C57BL/6 mice at days 0, 4, and 8 following intranasal inoculation with virus. Influenza-inoculated mice displayed a time-dependent reduction in both body weight and body-conditioning scores (Fig. 2 *A* and *B*) compared with saline-inoculated controls. As occurred in 2D2 inoculated mice, viral *M1* transcript was not detectable in cerebellar or spinal cord tissues, but was abundantly present in the lungs of infected animals (Fig. 2*C*, *Left*). Furthermore, we did not detect viral RNA in olfactory bulbs (Fig. 2*C*, *Right*), again confirming that this dose of virus does not infect the CNS. Nevertheless, RNA-sequencing analysis demonstrated changes in gene expression in both tissues due to infection (Fig. 2*D*). Although principal component analysis showed that the cerebellum and spinal cord are distinct at the transcriptome level, both tissues demonstrated time-dependent alterations of the transcriptome (Fig. 2*F*). After assigning a 1.5-fold change in expression and a false discovery rate (FDR) of <0.05 as a cutoff criteria, 21 annotated, differentially expressed genes (DEG) were identified in the cerebellum

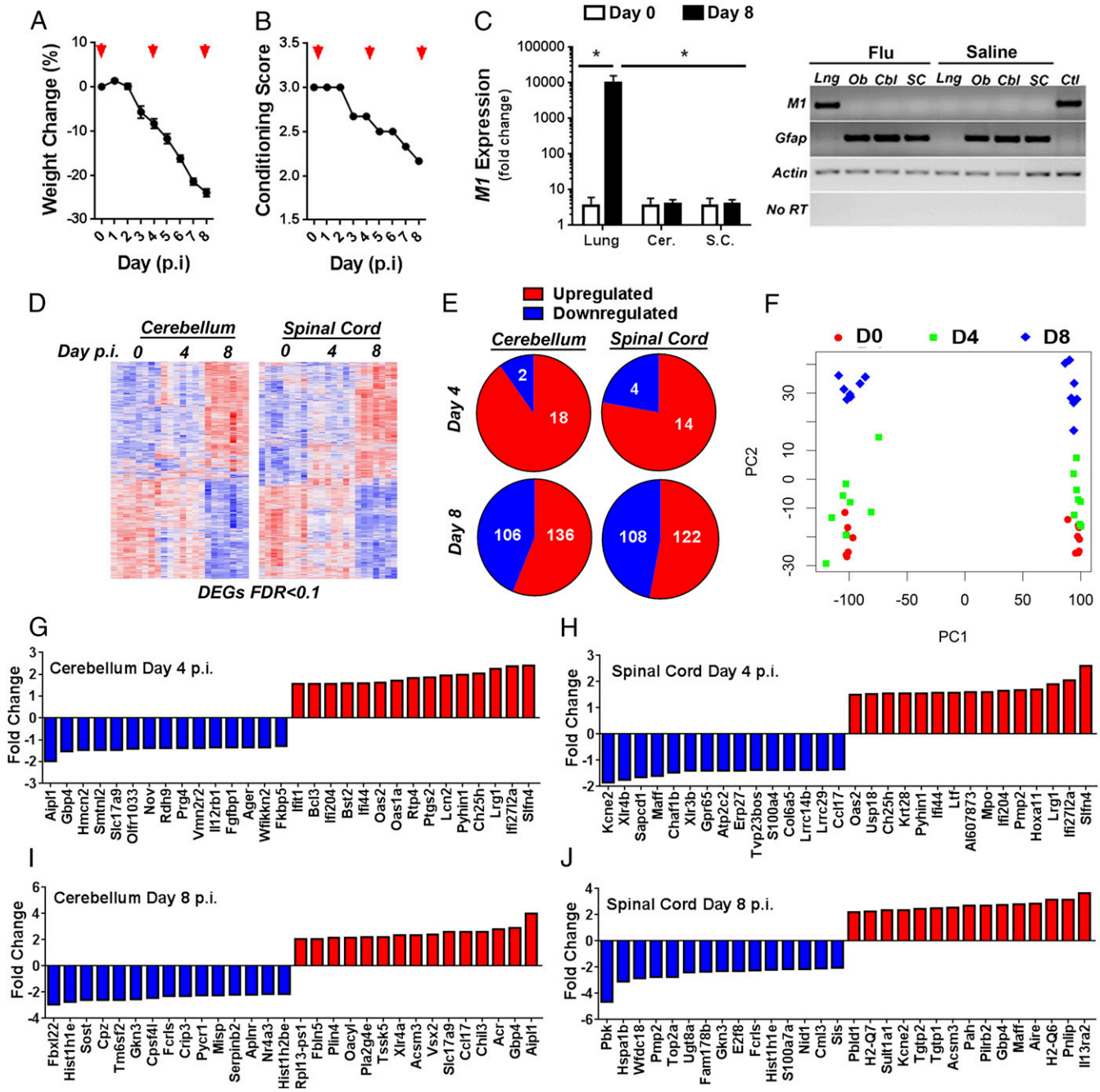

Fig. 2. Influenza infection induced alterations in the transcriptome. (*A–J*) Male and female C57BL/6 mice were inoculated with influenza (1.0 HAU) via the intranasal (i.n.) route. Mice were euthanized and RNA was isolated at days 0, 4, and 8 p.i. ($n = 7$–8 per time point). (*A* and *B*) Changes in body weight (*A*) and conditioning scores (*B*) over the course of infection. Results are expressed as means ± SE. Arrows depict tissue-collection time points. (*C*) Relative levels of viral *M1* in the CNS and lungs of control and virus-inoculated mice as determined by RT-qPCR (*Left*). Results are expressed as means ± SEM; $*P < 0.05$. At day 8 p.i., RNA was isolated from lungs (*Lng*), olfactory bulbs (*Ob*), cerebellum (*Cbl*), and spinal cords (*SC*) of influenza- and saline-inoculated mice converted to cDNA and amplified using primers specific for influenza *M1*, *Gfap*, and *Actin*. RNA that had not been reverse-transcribed to cDNA served as a negative control (*No RT*). Viral RNA served as a positive control (*Ctl*). Results are from one mouse from each experimental condition. (*D*) Heat maps showing DEGs in the cerebellum (*Left*) and spinal cord (*Right*) that result from infection (FDR < 0.01). (*E*) The numbers of up-regulated genes in the cerebellum (*Left*) and spinal cord (*Right*) at day 4 (*Top*) and day 8 p.i. (*Bottom*) assuming >1.5-fold change and FDR < 0.05. (*F*) Principal component analysis demonstrating differences between tissue (PC1) and day p.i. (PC2). Data for individual mice at day 0 (*red*), 4 (*green*), and 8 (*blue*) are shown. (*G–J*) The top annotated up-regulated and down-regulated genes in the cerebellum (*Left*) and spinal cord (*Right*) at day 4 (*Top*) and day 8 p.i. (*Bottom*).

and 18 DEGs in the spinal cord at day 4 p.i. compared with day 0. At day 8 p.i., there were 242 and 230 DEGs in the cerebellum and spinal cord, respectively (Fig. 2*E*). The top 30 DEGs in the cerebellum and spinal cord at days 4 (Fig. 2 *G* and *H*) and 8 (Fig. 2 *I* and *J*) are shown.

Infection Up-Regulates Genes Associated with Glial Activation. Peripheral injection of poly(I:C) or LPS up-regulates the expression of genes associated with the complement cascade in the CNS (27, 28). Interestingly, peripheral LPS injection is sufficient to induce an "A1" reactive astrocyte phenotype that is

dependent on microglial cell activation and C1qa, IL-1α, and TNF production (29). Therefore, we questioned if upper-respiratory viral infection was capable of altering genes associated with astrocyte activation. Both *C1qa* and *C1qb* genes were increased in the cerebellum at day 4 p.i. In the spinal cord, *C1qa*, *C1qb*, and *Il1a* were elevated but not significantly different from controls (Fig. 3*A*). However, *Lta* (which also signals to TNFR1) was up-regulated in the spinal cord at day 8 p.i. (Fig. 3*A*). *Tnf* was not detectable in either the brain or the spinal cord. Strikingly, most genes that were recently identified as predictors of an A1-reactive astrocyte phenotype were elevated in both cerebellar (9/12; Fig. 3*B*) and spinal cord tissues (11/11; Fig. 3*C*) at day 8 p.i. In contrast, fewer genes associated with an A2-reactive astrocyte profile were increased in cerebellar (3/9) and spinal cord tissue (3/10). Together, these data indicate that, similar to peripheral LPS injection, upper-respiratory infection promotes an A1 astrocyte phenotype in both brain and spinal cord (Fig. 3) and provides strong evidence that is suggestive of reactive gliosis.

Up-Regulated Genes Are Associated with IFN and MAPK Signaling During Infection. We next conducted bioinformatics analysis on genes that exhibited at least a 1.5-fold increase and an FDR of <0.05. Few genes met this criteria for up-regulation at day 4 p.i., but gene ontology (GO) analysis of the 18 up-regulated genes in the cerebellum identified terms associated with antiviral immunity as enriched (Fig. S3*A*). No gene ontology terms were enriched in the spinal cord, although cellular response to "interferon-beta signaling" and "positive regulation of osteoblast differentiation" were identified. Gene regulatory network analysis indicated that 72% of up-regulated genes in the cerebellum were targets of the transcription factor IFN regulatory factor 7 (IRF7; Fig. S3 *B* and *E*). Identical analysis of up-regulated genes in the spinal cord genes identified signal transducer and activator of transcription (STAT)1 as a regulator of expression (Fig. S3 *C* and *F*). Interestingly, the most enriched transcription factor-binding motif from genes in both tissues was identical (Fig. S3*D*).

Because IRF7 and STAT1 are activated in response to IFN receptor signaling, we questioned which of the observed up-regulated genes in the CNS are targets of IFN signaling using the database Interferome. All up-regulated genes in the cerebellum (18/18) and 85.7% (12/14) of genes in the spinal cord are known to be induced by IFN signaling. In the cerebellum, 36.8% (7/19) were identified as activated by type I interferons, whereas the remaining 63.15% were identified as products of either type I or type II IFN signaling (Fig. S3*G*). In the spinal cord, 66.6% of IFN-inducible genes were suspected products of type I interferons, whereas the remaining 33.3% were shown to be induced by both type I and type II IFN receptor ligation (Fig. S3*H*). None of the genes have been shown to be induced by type III interferons. Type I IFN receptors are ubiquitously expressed, and *Ifnar1*, *Ifnar2*, *Ifngr1*, *Ifngr2*, and *Ifnlr1* transcripts were detectible in cerebellar and spinal cord tissues. However, we did not detect expression of *Ifna*, *Ifnb1*, *Il28a, Il28b*, or *Il29* transcripts. Overall, these data show that the most prominent up-regulated genes in the CNS during influenza infection are controlled by IFN signaling.

At day 8 p.i., gene ontology analysis of up-regulated genes in the cerebellum identified terms associated with immune system responses as enriched, although no terms reached statistical significance. In the spinal cord, the term "immune system process" was significantly enriched. After relaxing the criteria for up-regulation to include genes that exhibited a 1.4-fold increase and an FDR <0.05, the gene ontology terms relating to immune responses became significantly enriched in both CNS tissues (Fig. S4). Importantly, the examination of coexpressed up-regulated genes in these tissues that comprised the GO term "immune system response" as stipulated by our original criteria implicated IFN-γ signaling in controlling the expression of these inflammatory genes (Fig. 4*A*). However, as on day 4 p.i., IFN transcripts were undetectable within cerebellar or spinal cord

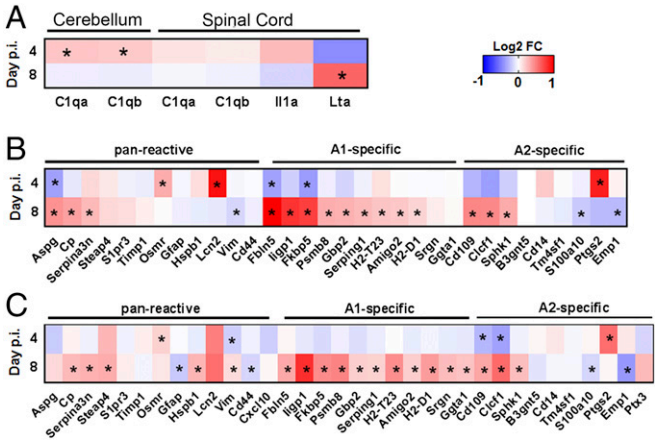

Fig. 3. Influenza infection up-regulates genes associated with reactive astrocytes. (*A*) Expression of genes associated with induction of A1 astrocytes in the cerebellum and spinal cord at day 4 (*Top*) and day 8 p.i. (*Bottom*) as determined from RNA-seq data. (*B* and *C*) Expression of pan-reactive, A1-specific, and A2-specific astrocyte genes in the cerebellum (*B*) and spinal cord (*C*) at day 4 and day 8 p.i. Data are means from seven to eight mice per group and are presented as log2 fold change from baseline (day 0). *, FDR < 0.05.

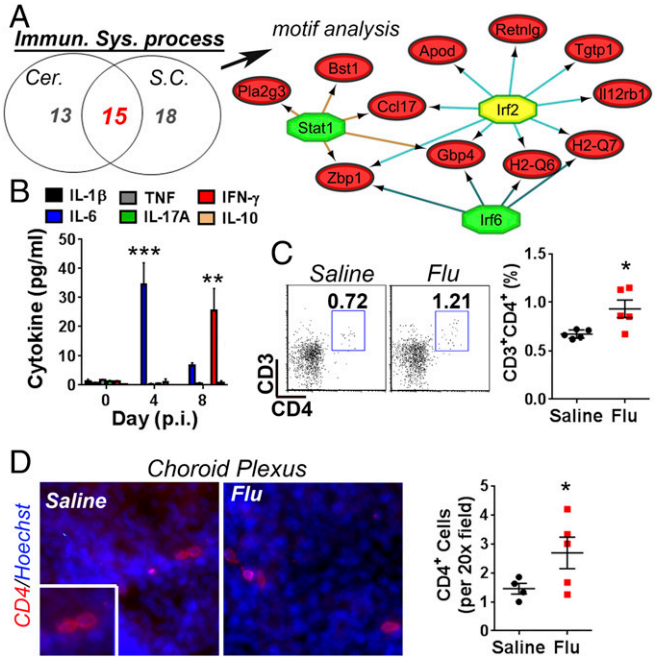

Fig. 4. Infection increases T-cells in the choroid plexus. (*A*) Numbers of genes comprising the gene ontology term "immune system process" in the cerebellum, spinal cord, or both (*Left*). Top three putative transcription factors identified by iRegulon analysis of coexpressed genes (*Right*). (*B*) Serum cytokines at days 0, 4, and 8 p.i. (n = 7–8 per time point). (*C*) Flow cytometry analysis of brain-infiltrating $CD3^+CD4^+$ after gating on viable and single cells at day 8 p.i. (n = 5 per group). (*D*) Immunofluorescent analysis showing $CD4^+$ cells in the choroid plexus of saline-inoculated and influenza-inoculated mice at day 8 p.i. Data in *D* represent the average of three to four images per mouse (n = 4–5 per group). Significance in *D* was determined using a one-tailed Student's t test. Data are means ± SE; $^*P < 0.05$, $^{**}P < 0.01$, $^{***}P < 0.001$.

tissues. These data indicate that signaling within the CNS may arise from a peripheral, potentially humoral source.

Influenza Infection Causes Immune Cell Surveillance of the CNS. We next analyzed serum cytokines in saline- and influenza-inoculated mice. Infection increased circulating levels of IL-6 (day 4 p.i.) and IFN-γ (day 8 p.i.) but had no effect on IL-1β, TNF, IL-17A, and IL-10 levels (Fig. 4*B*). Because IFN-γ signaling to the choroid plexus can promote T-cell surveillance of the CNS (9) and choroid plexus epithelial cells are accessible to blood cytokines, we conducted studies to determine if peripheral infection caused an influx of T-cells into the brain. Infection temporally increased the percentage and number of $CD3^+$ T-cells, but not $CD19^+$ B-cells, at day 8 p.i. in the brain (Fig. S5). Experimental replication confirmed an increased percentage of $CD3^+CD4^+$ helper T-cells (Fig. 4*C*) in the brains of influenza- vs. saline-inoculated mice at day 8 p.i. To determine if $CD4^+$ T cells localized to the choroid plexus, we isolated the choroid plexus of saline- and virus-inoculated mice at day 8 p.i. and then examined whole mounts by immunohistochemistry. The choroid plexus of influenza-infected mice contained more $CD4^+$ cells than saline-inoculated mice (Fig. 4*D*).

Several chemokines were up-regulated in the brain and spinal cords of influenza- vs. saline-inoculated controls (Fig. 5*A*). Specifically, influenza-inoculated mice had increased *Ccl17*, *Ccl25*, and *Ccl28*, but decreased *Ccl27a* and *Cx3cl1* expression in the cerebellum and spinal cords at day 8 p.i. Interestingly, peripheral infection up-regulated *Ccl6* and *Cxcl5* in the cerebellum, but not the spinal cord, at day 8 p.i. Both CCL17 and CCL28 are attractants for macrophages, dendritic cells, and Th2 cells, whereas CXCL5 is a monocyte and neutrophil chemoattractant and has been identified as a putative serum biomarker of MS relapse (30). Therefore, we questioned whether peripheral infection caused immune surveillance of the brain by innate immune cells. Infection did not alter the percentages of immune cells in the brain at either day 2 or 4 p.i. (Fig. S6 *A–C*). However, at day 8 p.i., we observed an increase in the percentage of lymphocytes ($CD45^{hi}CD11b^-$) and monocytes/neutrophils ($CD45^{hi}CD11b^+$) in the brains of infected mice (Fig. 5 *E* and *F* and Fig. S6 *C–E*). Further analysis indicated that the increase in myeloid lineage cells likely included a mixture of both inflammatory monocytes ($CD45^{hi}CD11b^+Ly6C^{hi}$) and neutrophils ($CD45^{hi}CD11b^+Gr\text{-}1^+Ly6C^{int}MHCII^-CD19^-$) (Fig. S6 *F* and *G*). However, the percentages of microglia ($CD45^{int}CD11b^+$) and dendritic cells ($CD11b^+CD11c^+$) did not differ between saline- and influenza-inoculated mice (Fig. S6*B* and Fig. 5 *B–H*). Importantly, percentages of lymphocytes in the blood and the brain differed substantially (Fig. 5*M*). Furthermore, these ratios differed among infected mice as well, indicating that residual cells from contaminating blood were not likely the source of immune cells isolated from the brain (see Fig. S7 for gating strategy).

Taken together, these data indicate that influenza infection causes an increase in immune cell surveillance of the brain and may implicate the choroid plexus as a potential entry site, although the data do not rule out extravasation across cerebrovascular endothelium or leptomeninges as additional and/or alternative routes.

Influenza Infection Modulates the Percentage of MHC Class II^+ B Cells in the CNS. T-cell reactivation in the CNS is partially attributed to B-cells (31, 32). Therefore, we next questioned if influenza infection altered the expression of MHC class II on B-cells. As reported previously, we found that B-cells were the major MHC class II-expressing cell in the naive mouse brain (31). Furthermore, we found that the expression of MHC class II on B-cells was higher on cells from infected mice at day 8 p.i. compared with controls (Fig. S8 *A–C*). As previously described (31), two populations of B-cells were present in the naive brain that were

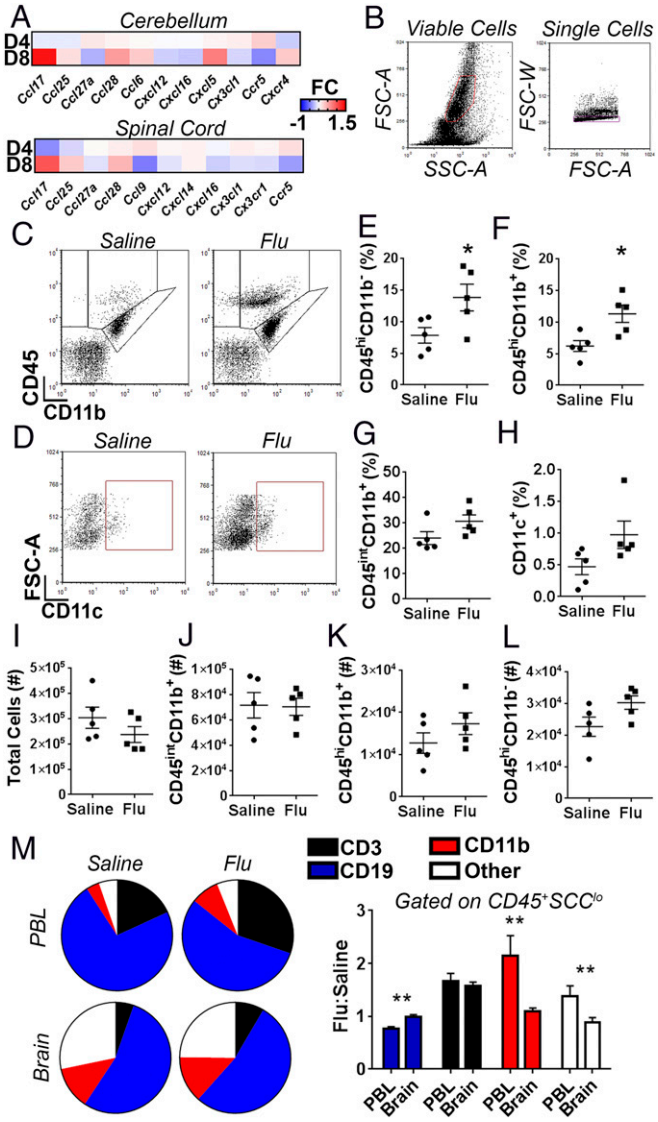

Fig. 5. Monocytes are increased in the brain during influenza infection. (*A*) Significantly up-regulated chemokines in the cerebellum (*Top*) and spinal cords (*Bottom*) of influenza-infected mice at days 4 (D4) and 8 (D8) p.i. as determined by RNA-seq. [Scale bar is log2 fold change (FC).] Data are representative of seven to eight mice per group. (*B–L*) C57BL/6 mice were inoculated with saline (n = 4–8) or influenza (1.0 HAU; n = 5–8). At day 8 p.i., mice were perfused with PBS and cells were isolated from the brain by percoll gradient centrifugation. The immunophenotype of isolated cells was determined by flow cytometry. All events were initially gated on viable and single cells. (*B–D*) Gating strategy used to determine lymphocytes ($CD45^{hi}CD11b^-$), monocytes/neutrophils ($CD45^{hi}CD11b^+CD11c^-$), and microglia ($CD45^{int}CD11b^+$) (*C*) and dendritic cells ($CD45^{hi}CD11c^+$) (*D*). (*E–H*) Effects of infection on percentage of lymphocytes (*E*), monocytes/neutrophils (*F*), microglia (*G*), and dendritic cells (*H*). The effect of infection on total cell numbers (*I*), microglia (*J*), myeloid cells (*K*), and lymphocytes (*L*). Results are means ± SE. Results from five mice per group are shown. (*M*) The percentages of leukocytes in the peripheral blood (PBL; *Top*) and in the brain (*Bottom*) at day 8 p.i. of saline- vs. influenza-inoculated mice are shown (*Left*). The effect of influenza infection on T-cell ($CD3^+$), B-cell ($CD19^+$), and macrophage ($CD11b^+SCC^{lo}$) is shown (*Right*). Gating strategy is shown in Fig. S6. Results are means ± SE from two to three independent experiments. Results are from four to eight mice per group. $^*P < 0.05$, $^{**}P < 0.01$.

distinguishable when gating on CD45 and CD19 (Fig. S5*C* and Fig. 6*A*). Infection did not alter the percentages or numbers of total $CD45^+CD19^+$ cells in the brain (Fig. 6*B*). However, the

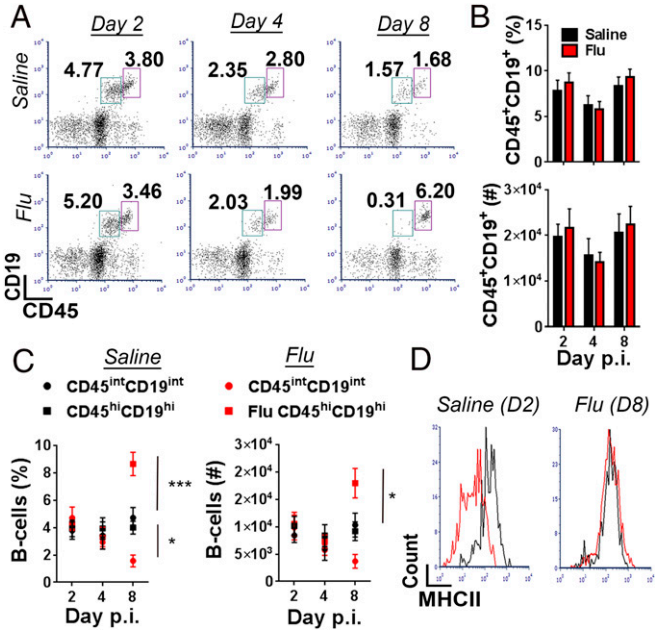

Fig. 6. Infection increases the percentage of MHC class II-expressing B-cells in the CNS. (*A–C*) C57BL/6 mice were inoculated with sterile saline or influenza (1.0 HAU) i.n. Immune cells were isolated from brains by percoll gradient centrifugation and subjected to flow cytometry. Events were gated on viable and single cells (Fig. S7). (*A*) Representative flow cytometry plots showing the effect of infection on $CD45^{int}CD19^{int}$ (*green*) and $CD45^{hi}CD19^{hi}$ (*purple*) populations in the brain at days 2, 4, and 8 p.i. (*B*) The effect of infection on B-cell ($CD45^{+}CD19^{+}$) percentage (*Top*) and the total number (*Bottom*) isolated from the brain. (*C*) The effect of infection on the percentages of $CD45^{int}CD19^{int}$ and $CD45^{hi}CD19^{hi}$ B-cell populations in the brain. (*D*) MHC class II expression on myeloid/microglia ($CD11b^{+}$) and B-cells ($CD19^{+}$) was examined during the course of infection. For gating strategy, see Fig. S7. Representative histogram showing mean fluorescent intensity of MHC class II stain on $CD45^{int}CD19^{int}$ (*red*) and $CD45^{hi}CD19^{hi}$ (*black*) populations in control mice at day 2 p.i. (*Left*). MHC class II mean fluorescent intensity on $CD45^{hi}CD19^{hi}$ B-cells from an infected mouse at day 2 (*black*) and day 8 (*red*) post infection. (*right*). Results in *D* are representative of three to five mice per group. Results in *A–C* are combined means ± SE from four independent experiments; n = 6–14 mice per group (day 2, n = 6–9; day 4, n = 7–9; day 8, n = 12–14 per group). $^{*}P < 0.05$, $^{***}P < 0.001$.

percentage of $CD45^{int}CD19^{int}$ B-cells decreased at day 8 p.i. In contrast, the percentage of $CD45^{hi}CD19^{hi}$ B-cells increased as a result of infection (Fig. 6*C*). Because $CD45^{hi}CD19^{hi}$ comprise the predominant MHC class II-expressing population in the murine brain (32) (Fig. 6*D*, *Left*), we questioned whether infection altered MHC class II expression on these cells. When gating on the $CD45^{hi}CD19^{hi}$ population of B-cells, the mean fluorescent intensity of MHC class II did not differ between saline- and influenza-inoculated mice at day 8 p.i. (Fig. 6*D*, *Right*). These data indicate that the observed change in B-cell MHC class II expression during infection is attributable to an increased percentage of $CD45^{hi}CD19^{hi}$ cells in the CNS rather than to an increased expression of surface MHC class II.

Both IFN-γ and CXCL5 Are Elevated in Cerebral Spinal Fluid of Patients During Relapse. We next questioned whether any of the chemokines that we identified as up-regulated in the CNS of mice during peripheral infection were increased in the cerebral spinal fluid samples of MS patients sampled during relapse vs. remission. The demographics of the patient population are shown in Table S1. Regardless of disease status, CXCL1, CXCL5, CXCL8, CCL27, CCL28, CXCL12, CX3CL1, and IFN-γ were detectable in patient cerebrospinal fluid (CSF) (Fig. 7 *A–H*). The chemokines CCL17 and CXCL2 were undetectable. The only chemokine that was significantly increased as a result of relapse was CXCL5 (Fig. 7*B*), although CXCL1 showed a trend toward being increased in the CSF during relapse (Fig. 7*A*; $P = 0.06$). Levels of IFN-γ were also elevated in MS patients during relapse (Fig. 7*H*).

Discussion

In this study, we investigated the ability of a mouse-adapted human influenza virus to trigger neurological disease in the autoimmune-prone TCR transgenic 2D2 mouse line. We found that infection with influenza virus is capable of causing both clinical and histological evidence of neurological disease. Additionally, we showed that peripheral influenza infection causes time-dependent transcriptomic changes to occur in both the cerebellum and the spinal cord that are consistent with the up-regulation of immune response genes, of which many are downstream of type I and type II IFN receptor signaling. Furthermore, we demonstrate that influenza infection potentiates immune cell surveillance of the CNS and identify CXCL5 as up-regulated in the CNS of animals during peripheral infection as well as in the CSF of MS patients during relapse. Collectively, these data indicate that upper-respiratory infection activates glia and potentially choroid plexus epithelial cells to promote immune cell trafficking to the CNS, which can, under the correct circumstances, trigger neurological disease.

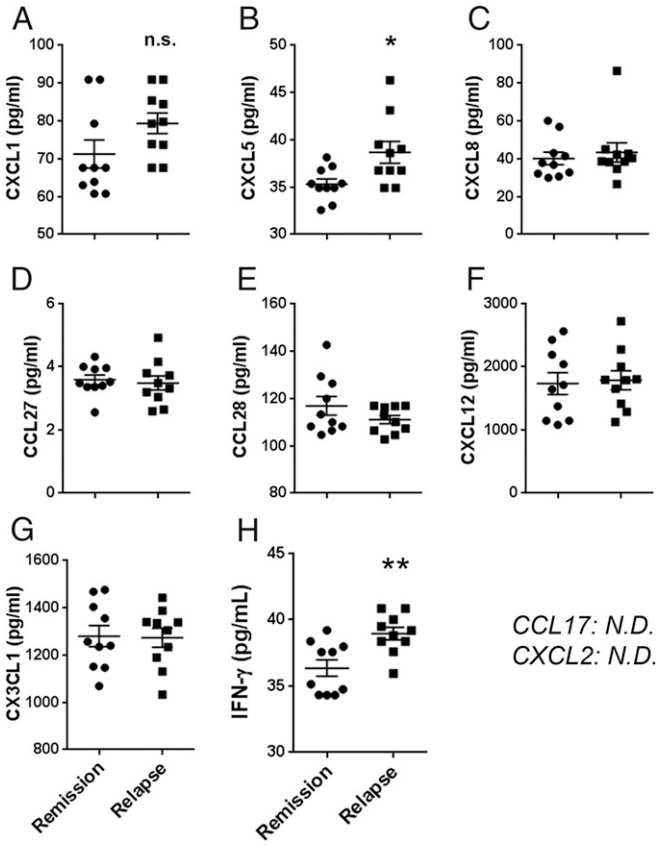

Fig. 7. CXCL5 levels are elevated in the cerebrospinal fluid of MS patients during relapse. (*A–G*) Levels of CXCL1 (*A*), CXCL5 (*B*), CXCL8 (*C*), CCL27 (*D*), CCL28 (*E*), CXCL12 (*F*), CX3CL1 (*G*), IFNγ (*H*), CCL17, and CXCL2 in the CSF of MS patients in remission (n = 10) and during relapse (n = 10) were measured by Luminex. Results are means ± SE. Mann–Whitney U tests were used to determine significance. $^{*}P < 0.05$, $^{**}P < 0.01$; n.s., not significant; N.D., not detectable.

Data originating from the majority (13–17, 21, 23, 24), but not all (33), studies that have investigated the relationship between upper-respiratory infection and MS exacerbation implicate viral infection as a trigger of relapse. Upper-respiratory infection by rhinovirus and enterovirus has been associated with MS relapse (13, 23). However, aside from picornaviruses, other viruses that infect the upper-respiratory tract have also been linked to exacerbation of inflammatory demyelinating disease. For example, in one case study, influenza infection caused relapse in a patient diagnosed with acute disseminated encephalomyelitis (34). Notably, several studies that examined the effects of upper-respiratory infection on MS relapse included "flu-like symptoms" and "fever over 38 °C" as criteria for occurrence of infection, indicating that influenza may have been the culprit underlying disease exacerbation in a few of these patients (14, 21, 24). That influenza is associated with exacerbation of MS symptoms is further eluded to by epidemiological data that link the incidence of MS hospitalizations to influenza epidemics (22). Moreover, De Keyser et al. have shown that influenza infection increases relapse risk whereas patients vaccinated against influenza had a lower risk of relapse (24). Many, but not all, studies have shown that influenza vaccination inhibits relapse (35). Thus, these data suggest that influenza infection may promote exacerbation of MS symptoms.

How viral infection contributes to relapse is not known, but it may involve up-regulation of inflammatory cytokines both peripherally and centrally within the CNS. It is established that peripheral injection of TLR agonists such as LPS, poly(I:C), and imiquimod promotes global changes in immune-responsive genes, including chemokines, within the CNS (1, 36). Likewise, influenza infection causes microglia activation and promotes the central up-regulation of proinflammatory cytokines and chemokines (4, 5, 37). Because s.c. injection of complete Freund's adjuvant (CFA) (8), cutaneous treatment with imiquimod (2), and upper-respiratory infection with *Bordetella pertussis* (38) each caused T-cell surveillance of the brain parenchyma, it is plausible that glial activation during peripheral inflammation is a catalyst for autoreactive T-cell attraction to the CNS. It is known that nonautoreactive activated T-cells traffic to the CNS (39–41), but what triggers this trafficking is still not completely defined. Cells residing in lung tissue may be unique in their ability to direct activated T-cells to the CNS as T-cells were shown to be licensed in this tissue to traffic to the brain and spinal cord (42). However, concurrent respiratory infection with *B. pertussis* inhibited EAE onset when the disease was actively induced with CFA (43). Furthermore, multiple autoimmune transgenic mouse lines are known to develop EAE following systemic injection of TLR agonists or pertussis toxin alone (25, 44, 45). As such, it is tempting to speculate that activation of resident CNS cells, in response to pathogen-specific peripheral inflammation, have a role in the trafficking of autoreactive T-cells to the CNS. In addition, we show that infection increases MHC class II+ B-cells in the brain. These data are important because B-cells are known to contribute to reactivation of T-cells during EAE (31, 32) and also contribute to relapse in MS (46). Therefore, uncovering the mechanisms governing the effect of peripheral infection on surveillance and reactivation is relevant not only to the pathogenesis of MS but also to many neuroinflammatory diseases.

Because all of the experiments were not conducted in 2D2 mice, which differ in their immune responsiveness to virus, it is likely that some of the observed responses that occurred in C57BL/6 mice would be different, particularly temporally in the 2D2 strain. Nevertheless, the data presented here add to the understanding of how systemic inflammation affects the CNS by demonstrating that peripheral infection with a live virus induces the up-regulation of IFN-responsive genes in the cerebellum and spinal cord. These data strongly agree with those from Thomson et al., which clearly show an effect of systemic TLR7 ligation and IFN gene induction in the brain (36). Notably, influenza viral RNA is recognized by TLR7 (47). In addition, we identified an association between circulating IFN-γ levels, type II IFN signaling in the brain, and immune cell surveillance. In our studies, these molecular events preceded the onset of neurological disease in 2D2 mice, which occurred within 2 wk of infection. As such, our findings are similar to what is observed in human MS patients following upper-respiratory infection in both incidence and timing of relapse after the occurrence of symptoms of upper-respiratory viral infection. In fact, MS patients are at higher risk for relapse within 2 wk before and 5 wk after the occurrence of sickness behaviors that are indicative of upper-respiratory infection. During this at risk period (ARP) MS patients were shown to have higher numbers of circulating IFN-γ producing cells compared with measurements taken outside of this time frame (21). It is also noteworthy that a single i.v. injection of IFN-γ triggered relapse in 38% (7/18) of MS patients (48). These IFN-γ–induced relapses lasted longer than 24 h and all occurred within the time frame that would be considered the ARP for an infection-induced relapse. Recently, Kunis et al. have provided compelling data suggesting that IFNGR signaling at the choroid plexus is needed for immune cell surveillance of the CNS (9). In relation to MS, these data are interesting because there is an association with IFN-γ signaling and relapse and also because this portal of T-cell entry into the CNS may partially explain the periventricular predilection of lesions in MS patients. As such, it is conceivable that circulating IFN-γ, resulting from peripheral infection, aids in the surveillance of the CNS by immune cells and that, under the correct circumstances, may be sufficient to stimulate autoimmune cell activation/reactivation and disease exacerbation. It is noteworthy that we found elevated levels of IFN-γ in patient CSF during relapse compared with samples taken during remission. Although IFN-γ is capable of promoting relapse in MS patients, its role in the pathogenesis of EAE has traditionally been ascribed as protective. However, more recent data suggest that the absence of IFN-γ signaling to brain glia promotes atypical signs of EAE and is associated with cerebellar pathology (49, 50).

An alternative hypothesis, which may not be mutually exclusive, is that peripheral infection-induced up-regulation of TNF and IL-1β within the CNS is required for disease initiation or relapse. The generation of classical EAE is dependent on the activation of microglial transforming growth factor beta (TGFβ) 1-activating kinase (TAK)1 activation, which is downstream of both IL-1β and TNFR1 receptor signaling (51). Furthermore, deletion of TAK1 signaling in Nestin$^+$ cells diminishes disease severity, indicating that IL-1β and TNF activation of microglia and/or astrocyte TAK1 likely induces chemokines needed to attract peripheral immune cells. It has been proposed that neutrophils are the source of IL-1β that is needed for EAE induction (52). These data are interesting because neutralizing antibodies directed against CXCR2 ameliorates atypical EAE, which was shown to be dependent on neutrophil recruitment (50, 53). Furthermore, atypical EAE was strongly linked to astrocyte production of the CXCR2 ligands CXCL1, CXCL2, and CXCL5 (50). These data are relevant because (*i*) serum CXCL5 was recently reported to be a prognostic factor for MS relapse (30) and (*ii*) we now show that CXCL5 is increased in the CSF of MS patients during relapse. In the current study, we observed demyelination in the cerebellum of several infected 2D2 transgenic mice and increased surveillance of the brain by monocytes and neutrophils, and our transcriptomic analysis identified *Ccl17*, *Ccl6*, and *Cxcl5* as up-regulated in the cerebellum as a result of peripheral infection. These chemokines were previously identified as highly expressed in atypical vs. classical EAE (54). We did not detect CCL17 in CSF of MS patients and did not observe increased levels of either CCL27 or CCL28 during relapse. These results do not necessarily exclude the involvement of these

chemokines in the pathogenesis of MS, especially given our small sample size. However, that CXCL5 was increased during relapse supports the role of this chemokine in the pathogenesis of relapse, and it is tempting to speculate that the production of this chemokine within the CNS parenchyma by peripheral inflammation facilitates relapse.

In conclusion, we found that intranasal inoculation with influenza A virus facilitated glial activation and immune surveillance and was sufficient to induce neurological and histological disease in autoimmune-prone 2D2 transgenic mice. Comparisons between peripheral infection induced neuroinflammation as determined by gene expression and human cytokine, and chemokine levels during relapse indicate that up-regulation of IFN-γ signaling during infection may contribute to relapse. These observations contribute to a better understanding of how peripheral infection may act to exacerbate neurological diseases such as multiple sclerosis and potentially others.

Materials and Methods

Mice. Eight- to 12-wk-old male and female mice were used for these studies. All mice were originally obtained from Jackson Laboratory. Mice used for these experiments included wild-type C57BL/6J (catalog no. 000664) and C57BL/6-Tg(Tcra2D2,Tcrb2D2)1Kuch/J (2D2; catalog no. 006912). All animals were housed under constant 12-h light/dark cycles and constant temperature and fed with a standard rodent diet ad libitum. The experimental procedures described here were approved by the Institutional Animal Care and Use Committee at the University of Illinois Urbana–Champaign and were performed in accordance with guidelines of the National Institutes of Health.

Intranasal Viral Infection and Behavioral Indices of Sickness. Mice were anesthetized with 4% isoflurane and then inoculated with either sterile saline or mouse-adapted human influenza A virus (strain A/Puerto Rico/8/1934 H1N1; PR8) diluted in sterile PBS in a total volume of 50 μL. Body weights and conditioning scores were recorded daily. Body-conditioning scores were assessed as follows: Score 1 is an emaciated mouse with skeletal structure extremely prominent and vertebrae distinctly segmented; score 2 is an under-conditioned mouse with segmentation of vertebral column evident and pelvic bones readily palpable; score 3 is a well-conditioned mouse with nonprominent vertebrae and pelvis; score 4 is an overconditioned mouse characterized by vertebrae that are palpable only with firm pressure; and score 5 is an obese mouse. Clinical signs of EAE were recorded as reported previously (55). In brief, score 0, no abnormalities detected; 0.5, weak tail; 1, tail paralysis; 2, loss of coordinated movement and hind-limb paresis and/or decreased righting reflex; 3, paralysis of one hind limb; 4, paralysis of both hind limbs; 4.5, paralysis of both hind limbs and forelimb weakness; 5, moribund. When a mouse received a score for EAE this score was confirmed by a blinded rater.

RNA Isolation, cDNA Library Generation, and RT-qPCR. At days 0 (noninfected), 4, and 8 p.i., mice were brought to a surgical plane of anesthesia by i.p. injection of mixture of ketamine (100 mg/kg) and xylazine (10 mg/kg). Next, blood was collected from the heart, and then the mice were transcardially perfused with sterile PBS (pH 7.4). The cerebellum and the spinal cord were dissected, placed in RNAlater (Ambion), and transferred to −80 °C until use. The tissue was then homogenized by sonication, and total RNA was isolated by Tri reagent according to the manufacturer's instructions (Sigma). Samples were further purified using Thermojet RNA purification columns (ThermoScientific). Residual DNA was digested using DNaseI. The quality of RNA was checked for genomic DNA by gel electrophoresis on a 1.5% agarose gel. For each sample, strand-specific RNAseq libraries were prepared using TruSeq Stranded RNA sample prep kits (Illumina). Both PCR and qPCR were used to determine relative expression of viral *M1*, *Gfap*, *Actin*, and *Gapdh* using the following primer sequences: *M1*—Fwd-AAGACCAATCCTGTCACCTCTGA, Rev-CAAAGCGTCTAC GCTGCAGTCC; *Gapdh*—Fwd-GCATCTTCTTGTGCAGTGCC, Rev-TACGGCCAAATCCGTTCACA; *Gfap*—Fwd-CAGCTTCGAGCCAAGGAG, Rev-TGTCCC TCTCCACCTCCA; and *β-actin*—Fwd-AGACTTCGAGCAGGAGATGG, Rev-CAACGTCAC ACTTCATGATGG. Quantitative PCR was performed using Sybergreen (Bio-Rad) on a Step One Plus Real-Time PCR System (Applied Biosystem). Fold change in gene expression was calculated using the formula $2^{-\Delta\Delta Ct}$.

RNA-Sequencing and Data Analysis. RNA-seq data and statistical analyses were performed by the Roy J. Carver Bioinformatics Center (University of Illinois Urbana–Champaign). In brief, equimolar concentrations of libraries were pooled and then quantitated by qPCR. Next, the samples were subjected to 100-bp paired-end sequencing for 101 cycles on a HiSeq2500 using the HiSeq SBS sequencing kit version 4. Fastq files were generated and demultiplexed with the bcl2fastq v1.8.4 Conversion Software (Illumina). Trimmomatic (version 0.33) was used to trim any residual adapter content and low-quality bases. Sequences were aligned to the mouse (*Mus musculus*) genome using STAR (version 2.5.0a). Gene counts were determined using featureCounts (version 1.4.3-pl), and multimapping reads were excluded. After trimming and excluding multimapping reads, an average of 92.07 ± 0.09% (cerebellum) and 91.71 ± 0.23% (spinal cord) were uniquely mapped to a gene. The average number of single 100-bp paired-end gene reads obtained per sample was 72.04 million and 71.76 million in the cerebellum and spinal cord, respectively. The RNA sequencing datasets associated with this paper have been deposited into the Gene Expression Omnibus database (https://www.ncbi.nlm.nih.gov/geo/) and can be accessed using the accession no. GSE96870.

Gene ontology and pathway analyses were performed on up-regulated genes using DAVID Bioinformatics Researches 6.8(Beta) (https://david-d.ncifcrf.gov/). Predicted transcriptional regulators were identified using the iRegulon application in Cytoscape (56). For these analyses, the default settings of the program were used. For any given set of genes, putative transcription factors or motifs that achieved a normalized enrichment score of <3.0 and an FDR of >0.001 were considered to be potential regulators.

Serum Cytokine Measurements. Serum levels of TNF, IL-1β, IFN-γ, IL-6, IL-10, and IL-17A were determined by Bio-plex (Bio-Rad) using a luminex magnetic bead panel kit (Millipore) following the manufacturer's instructions.

Tissue-Specific Lymphocyte Extraction and Flow Cytometry. Mice were brought to a surgical plane of anesthesia by i.p. injection with ketamine (100 mg/kg) and xylazine (10 mg/kg) and then perfused with 10–20 mL of sterile PBS. The brain was removed, minced with a sterile razor blade, digested in StemPro Accutase buffer (Gibco) for 45 min at 37 °C, and then passed through a 70-μm filter (Corning) to remove debris. CNS-infiltrating lymphocytes were isolated by percoll gradient centrifugation as described previously (57). After washing, the cells were suspended in ice-cold staining buffer (sterile PBS containing 2% FBS). For experiments shown in Figs. 1 and 6 and Fig. S5, cells were blocked with anti-CD16/32 (clone 93) on ice for 10 min. Blocking antibody was not used for experiments shown in Figs. 4 and 5 and Fig. S4. Nevertheless, very similar results were obtained between experiments (Fig. S6*E*). The following antibody clones and conjugated fluorophores were used for phenotypical analysis: anti–CD3-eFluor450 (clone: 17A2), anti–CD3-PE-Cy7 (clone: 145–2C11), anti–CD4-eFluor450 (clone: GK1.5), anti–CD4-APC (clone: GK1.5), anti–CD4-FITC (clone: GK1.5), anti–CD8-PE-cy5.5 (clone: 53–6.7), anti–CD19-PE (clone: eBio1D3), anti–CD19-APC (clone: eBio1D3), anti–CD45-APC (clone: 30-F11), anti–CD45-PE (clone: 30-F11), anti–CD11b-FITC (clone: M170), anti–CD11c-eFluor450 (clone: N418), anti–MHCII-eFluor450 (clone: M5/114.15.2), anti–MHCII-APC (clone: H1519), anti–Vα3.2-APC (clone: RR3-16), anti–Vα3.2-eFluor450 (clone: RR3-16), anti–Ly6G/C-PE-Cy7 (clone RB6-HC5), and anti–Ly6C-PE-Cy5.5 (clone HK1.4) were all from eBioscience. After blocking, 5×10^5 cells were suspended in 0.1 mL of ice-cold staining buffer and stained on ice in the dark for 20 min. After washing twice in staining buffer, the samples were acquired on a LSRII Flow cytometer (BD). Gates were determined using unstained and single-stained samples obtained from the same tissue of origin. Results were analyzed using FCS Express 4 and 6 flow cytometry software (De Novo Software).

Histochemistry, Immunohistochemistry, and Tissue Analysis. Mice were brought to a surgical plane of anesthesia and then transcardially perfused with PBS. Brains and spinal columns were dissected and fixed in 10% neutral buffered formalin, paraffin embedded, and then sectioned in the sagittal (brain) and transverse (spinal cord) planes, using a microtome, and then stained with either H&E or luxol fast blue by the histopathology core facility at the University of Illinois Urbana–Champaign. Lesions were identified by an observer blinded to the experimental group. Representative images were collected using a NanoZoomer slide scanner (Hamamatsu Photonics).

In some experiments, the choroid plexus was isolated as previously described (58), fixed, mounted onto glass slides, and blocked with PBS containing 0.3% Triton-X 100 and 5% goat serum for 1 h at room temperature. T-cells were stained using a rat anti-mouse CD4 antibody (clone RM4-5; eBioscience) diluted 1:1,000 in PBS containing 0.1% Triton-X 100 (PBST) overnight at 4 °C. After washing, the tissue was incubated with an Alexa

Fluor 594-conjugated anti-rat IgG secondary diluted 1/1,000 in PBST at room temperature (RT). Hoechst 33342 trihydrochloride (1:2,000 Life Technologies) was then added for 1 min at RT to stain nuclei. The tissue was coversliped with flouromount-G (Southern Biotech) and imaged using a fluorescent microscope ZOE (Bio-Rad).

Human Cerebrospinal Fluid Samples. Human cerebrospinal fluid specimens were obtained from the Human Brain and Spinal Fluid Resource Center, VA West Los Angeles Healthcare Center, Los Angeles, CA 90073, which is sponsored by National Institute of Neurological Disorders and Stroke/National Institute of Mental Health, the National Multiple Sclerosis Society, and the Department of Veteran Affairs. Fluids were de-identified before acquisition. As such, Institutional Review Board approval was not necessary. Cerebrospinal fluids from MS patients in remission ($n = 10$) and in relapse ($n = 10$) were used to measure CXCL1, CXCL2, CXCL5, CXCL8, CXCL12, CCL17, CCL27, CCL28, CX3CL1, and IFN-γ levels by Luminex array according to the manufacturer's instructions (R&D Systems). All available information regarding human samples is shown in Table S1.

Statistical Analysis. Where appropriate, data were analyzed using one or two-tailed Student's *t* tests for comparisons between two groups as indicated in the figure legend. In the case of nonparametric analyses between two groups, data were analyzed by Wilcoxon rank-sum tests. The incidence of EAE onset was determined using χ^2 analysis. Because no saline-inoculated animals developed EAE, the known incidence of spontaneous EAE (4%) was used as a reference for controls (25). When comparing more than two groups, data were analyzed using multivariate analysis of variance followed by Bonferroni's post hoc test. Differences in survival were assessed using a log-rank Mantel–Cox test. GraphPad Prism (GraphPad Software) was used for statistical analysis. In all cases, $P < 0.05$ was considered significant.

ACKNOWLEDGMENTS. We thank Dr. Robert McCusker for allowing us to use his equipment and Dr. Mark Lawson for demonstrating intranasal inoculation procedures. We thank Dr. Barbara Pilas at the Roy J. Carver Biotechnology Center for her assistance with the flow cytometry. This research was funded in part by the National Multiple Sclerosis Society Pilot Grant PP3436 (to A.J.S. and R.W.J.); US Department of Agriculture, National Institute of Food and Agriculture, the HATCH Project 1005145 (A.J.S.); and University of Illinois start-up funds (A.J.S.).

1. Konat GW, Borysiewicz E, Fil D, James I (2009) Peripheral challenge with double-stranded RNA elicits global up-regulation of cytokine gene expression in the brain. *J Neurosci Res* 87:1381–1388.
2. McColl A, Thomson CA, Nerurkar L, Graham GJ, Cavanagh J (2016) TLR7-mediated skin inflammation remotely triggers chemokine expression and leukocyte accumulation in the brain. *J Neuroinflammation* 13:102.
3. Sandiego CM, et al. (2015) Imaging robust microglial activation after lipopolysaccharide administration in humans with PET. *Proc Natl Acad Sci USA* 112:12468–12473.
4. Jurgens HA, Amancherla K, Johnson RW (2012) Influenza infection induces neuroinflammation, alters hippocampal neuron morphology, and impairs cognition in adult mice. *J Neurosci* 32:3958–3968.
5. Sadasivan S, Zanin M, O'Brien K, Schultz-Cherry S, Smeyne RJ (2015) Induction of microglia activation after infection with the non-neurotropic A/CA/04/2009 H1N1 influenza virus. *PLoS One* 10:e0124047.
6. Ji P, Schachtschneider KM, Schook LB, Walker FR, Johnson RW (2016) Peripheral viral infection induced microglial sensome genes and enhanced microglial cell activity in the hippocampus of neonatal piglets. *Brain Behav Immun* 54:243–251.
7. Blank T, et al. (2016) Brain endothelial- and epithelial-specific interferon receptor chain 1 drives virus-induced sickness behavior and cognitive impairment. *Immunity* 44:901–912.
8. Schmitt C, Strazielle N, Ghersi-Egea JF (2012) Brain leukocyte infiltration initiated by peripheral inflammation or experimental autoimmune encephalomyelitis occurs through pathways connected to the CSF-filled compartments of the forebrain and midbrain. *J Neuroinflammation* 9:187.
9. Kunis G, et al. (2013) IFN-γ-dependent activation of the brain's choroid plexus for CNS immune surveillance and repair. *Brain* 136:3427–3440.
10. Holmes C, Cunningham C, Zotova E, Culliford D, Perry VH (2011) Proinflammatory cytokines, sickness behavior, and Alzheimer disease. *Neurology* 77:212–218.
11. Holmes C, et al. (2003) Systemic infection, interleukin 1beta, and cognitive decline in Alzheimer's disease. *J Neurol Neurosurg Psychiatry* 74:788–789.
12. Ferrari CC, Tarelli R (2011) Parkinson's disease and systemic inflammation. *Parkinsons Dis* 2011:436813.
13. Kriesel JD, White A, Hayden FG, Spruance SL, Petajan J (2004) Multiple sclerosis attacks are associated with picornavirus infections. *Mult Scler* 10:145–148.
14. Buljevac D, et al. (2002) Prospective study on the relationship between infections and multiple sclerosis exacerbations. *Brain* 125:952–960.
15. Edwards S, Zvartau M, Clarke H, Irving W, Blumhardt LD (1998) Clinical relapses and disease activity on magnetic resonance imaging associated with viral upper respiratory tract infections in multiple sclerosis. *J Neurol Neurosurg Psychiatry* 64:736–741.
16. Sibley WA, Bamford CR, Clark K (1985) Clinical viral infections and multiple sclerosis. *Lancet* 1:1313–1315.
17. Sibley WA, Foley JM (1965) Infection and immunization in multiple sclerosis. *Ann N Y Acad Sci* 122:457–466.
18. Compston A, Coles A (2008) Multiple sclerosis. *Lancet* 372:1502–1517.
19. Goodin DS, et al. (2016) Relapses in multiple sclerosis: Relationship to disability. *Mult Scler Relat Disord* 6:10–20.
20. De Keyser J, Zwanikken CM, Zorgdrager A, Oenema D, Boon M (1999) Treatment of acute relapses in multiple sclerosis at home with oral dexamethasone: A pilot study. *J Clin Neurosci* 6:382–384.
21. Correale J, Fiol M, Gilmore W (2006) The risk of relapses in multiple sclerosis during systemic infections. *Neurology* 67:652–659.
22. Oikonen M, et al. (2011) Temporal relationship between environmental influenza A and Epstein-Barr viral infections and high multiple sclerosis relapse occurrence. *Mult Scler* 17:672–680.
23. Kriesel JD, Sibley WA (2005) The case for rhinoviruses in the pathogenesis of multiple sclerosis. *Mult Scler* 11:1–4.
24. De Keyser J, Zwanikken C, Boon M (1998) Effects of influenza vaccination and influenza illness on exacerbations in multiple sclerosis. *J Neurol Sci* 159:51–53.
25. Bettelli E, et al. (2003) Myelin oligodendrocyte glycoprotein-specific T cell receptor transgenic mice develop spontaneous autoimmune optic neuritis. *J Exp Med* 197:1073–1081.
26. Kazmierski R, Wender M, Guzik P, Zielonka D (2004) Association of influenza incidence with multiple sclerosis onset. *Folia Neuropathol*. 42:19–23.
27. Michalovicz LT, Lally B, Konat GW (2015) Peripheral challenge with a viral mimic upregulates expression of the complement genes in the hippocampus. *J Neuroimmunol* 285:137–142.
28. Zamanian JL, et al. (2012) Genomic analysis of reactive astrogliosis. *J Neurosci* 32:6391–6410.
29. Liddelow SA, et al. (2017) Neurotoxic reactive astrocytes are induced by activated microglia. *Nature* 541:481–487.
30. Rumble JM, et al. (2015) Neutrophil-related factors as biomarkers in EAE and MS. *J Exp Med* 212:23–35.
31. Pierson ER, Stromnes IM, Goverman JM (2014) B cells promote induction of experimental autoimmune encephalomyelitis by facilitating reactivation of T cells in the central nervous system. *J Immunol* 192:929–939.
32. Parker Harp CR, et al. (2015) B cell antigen presentation is sufficient to drive neuroinflammation in an animal model of multiple sclerosis. *J Immunol* 194:5077–5084.
33. Kneider M, et al. (2015) Upper respiratory infections and MRI activity in relapsing-remitting multiple sclerosis. *Neuroepidemiology* 45:83–89.
34. Athauda D, Andrews TC, Holmes PA, Howard RS (2012) Multiphasic acute disseminated encephalomyelitis (ADEM) following influenza type A (swine specific H1N1). *J Neurol* 259:775–778.
35. Mokhtarian F, et al. (1997) Influenza virus vaccination of patients with multiple sclerosis. *Mult Scler* 3:243–247.
36. Thomson CA, McColl A, Cavanagh J, Graham GJ (2014) Peripheral inflammation is associated with remote global gene expression changes in the brain. *J Neuroinflammation* 11:73.
37. Jang H, et al. (2012) Inflammatory effects of highly pathogenic H5N1 influenza virus infection in the CNS of mice. *J Neurosci* 32:1545–1559.
38. McManus RM, Higgins SC, Mills KH, Lynch MA (2014) Respiratory infection promotes T cell infiltration and amyloid-β deposition in APP/PS1 mice. *Neurobiol Aging* 35:109–121.
39. Hickey WF, Hsu BL, Kimura H (1991) T-lymphocyte entry into the central nervous system. *J Neurosci Res* 28:254–260.
40. Smorodchenko A, et al. (2007) CNS-irrelevant T-cells enter the brain, cause blood-brain barrier disruption but no glial pathology. *Eur J Neurosci* 26:1387–1398.
41. Schläger C, et al. (2016) Effector T-cell trafficking between the leptomeninges and the cerebrospinal fluid. *Nature* 530:349–353.
42. Odoardi F, et al. (2012) T cells become licensed in the lung to enter the central nervous system. *Nature* 488:675–679.
43. Edwards SC, Higgins SC, Mills KH (2015) Respiratory infection with a bacterial pathogen attenuates CNS autoimmunity through IL-10 induction. *Brain Behav Immun* 50:41–46.
44. Goverman J, et al. (1993) Transgenic mice that express a myelin basic protein-specific T cell receptor develop spontaneous autoimmunity. *Cell* 72:551–560.
45. Waldner H, Collins M, Kuchroo VK (2004) Activation of antigen-presenting cells by microbial products breaks self tolerance and induces autoimmune disease. *J Clin Invest* 113:990–997.
46. Hauser SL, et al.; HERMES Trial Group (2008) B-cell depletion with rituximab in relapsing-remitting multiple sclerosis. *N Engl J Med* 358:676–688.
47. Diebold SS, Kaisho T, Hemmi H, Akira S, Reis e Sousa C (2004) Innate antiviral responses by means of TLR7-mediated recognition of single-stranded RNA. *Science* 303:1529–1531.
48. Panitch HS, Hirsch RL, Haley AS, Johnson KP (1987) Exacerbations of multiple sclerosis in patients treated with gamma interferon. *Lancet* 1:893–895.
49. Miller NM, Wang J, Tan Y, Dittel BN (2015) Anti-inflammatory mechanisms of IFN-γ studied in experimental autoimmune encephalomyelitis reveal neutrophils as a potential target in multiple sclerosis. *Front Neurosci* 9:287.

50. Simmons SB, Liggitt D, Goverman JM (2014) Cytokine-regulated neutrophil recruitment is required for brain but not spinal cord inflammation during experimental autoimmune encephalomyelitis. *J Immunol* 193:555–563.
51. Goldmann T, et al. (2013) A new type of microglia gene targeting shows TAK1 to be pivotal in CNS autoimmune inflammation. *Nat Neurosci* 16:1618–1626.
52. Lévesque SA, et al. (2016) Myeloid cell transmigration across the CNS vasculature triggers IL-1β-driven neuroinflammation during autoimmune encephalomyelitis in mice. *J Exp Med* 213:929–949.
53. Stoolman JS, Duncker PC, Huber AK, Segal BM (2014) Site-specific chemokine expression regulates central nervous system inflammation and determines clinical phenotype in autoimmune encephalomyelitis. *J Immunol* 193:564–570.
54. Stromnes IM, Cerretti LM, Liggitt D, Harris RA, Goverman JM (2008) Differential regulation of central nervous system autoimmunity by T(H)1 and T(H)17 cells. *Nat Med* 14:337–342.
55. Klaren RE, et al. (2016) Effects of exercise in a relapsing-remitting model of experimental autoimmune encephalomyelitis. *J Neurosci Res* 94:907–914.
56. Janky R, et al. (2014) iRegulon: From a gene list to a gene regulatory network using large motif and track collections. *PLOS Comput Biol* 10:e1003731.
57. Steelman AJ, et al. (2009) Restraint stress modulates virus specific adaptive immunity during acute Theiler's virus infection. *Brain Behav Immun* 23:830–843.
58. Bowyer JF, et al. (2012) A visual description of the dissection of the cerebral surface vasculature and associated meninges and the choroid plexus from rat brain. *J Vis Exp* (69):e4285.